The Astrophysical Journal, 574:104–113, 2002 July 20

THE LUMINOSITY FUNCTIONS AND STELLAR MASSES OF GALACTIC DISKS AND SPHEROIDS

A. J. Benson,[1] C. S. Frenk,[2] and R. M. Sharples[2]
Received 2001 November 7; accepted 2002 March 28

ABSTRACT

We present a method to obtain quantitative measures of galaxy morphology and apply it to a spectroscopic sample of field galaxies in order to determine the luminosity and stellar mass functions of galactic disks and spheroids. For our sample of approximately 600 galaxies, we estimate, for each galaxy, the bulge-to-disk luminosity ratio in the *I* band using a two-dimensional image fitting procedure. Monte Carlo simulations indicate that reliable determinations are only possible for galaxies approximately 2 mag brighter than the photometric completeness limit, leaving a sample of 90 galaxies with well-determined bulge-to-total light ratios. Using our measurements of individual disk and bulge luminosities for these 90 galaxies, we construct the luminosity functions of disks and spheroids and, using a stellar population synthesis model, we estimate the stellar mass functions of each of these components. The disk and spheroid luminosity functions are remarkably similar, although our rather small sample size precludes a detailed analysis. We do, however, find evidence in the bivariate luminosity function that spheroid-dominated galaxies occur only among the brightest spheroids, while disk-dominated galaxies span a much wider range of disk luminosities. Remarkably, the total stellar mass residing in disks and spheroids is approximately the same. For our sample (which includes galaxies brighter than $M_* + 2$, where M_* is the magnitude corresponding to the characteristic luminosity), we find the ratio of stellar masses in disks and spheroids to be 1.3 ± 0.2. This agrees with the earlier estimates of Schechter & Dressler but differs significantly from that of Fukugita, Hogan, & Peebles. Ongoing large photometric and redshift surveys will lead to a large increase in the number of galaxies to which our techniques can be applied and thus to an improvement in the current estimates.

Subject headings: galaxies: bulges — galaxies: luminosity function, mass function — galaxies: spiral

1. INTRODUCTION

It has long been known that galaxies in the nearby universe display a range of morphological characteristics that distinguish between disk-dominated (e.g., spiral) and spheroid-dominated (e.g., elliptical) galaxies, with many fine subdivisions within each class (e.g., Hubble 1926; de Vaucouleurs 1959). The origins of these different types of galaxy and the evolutionary connections, if any, between them are still unclear, although there is a wealth of observational data and several proposed theories.

Traditionally, morphology has been assigned by human classifiers directly from galaxy images, a process that is accurate only to within about two T-types (Naim et al. 1995). More recently, computer-based algorithms have been developed that show a reasonable correlation with "eyeball" estimates, at least for bright galaxies (e.g., Abraham et al. 1996). Unfortunately, all these classifications tend to give considerable weight to detailed morphological features, such as spiral arms or asymmetries in the image, and are difficult to compare with current theoretical predictions that focus on simpler quantities such as the total stellar mass or luminosity in the disk and spheroidal components. Here we consider a morphological quantifier that is more easily related to theoretical models.

It is widely believed that disks form by slow accretion of gas that acquired angular momentum through tidal torques (Hoyle 1949; Peebles 1969), although whether this picture works in detail remains an open question (Navarro, Frenk, & White 1995; Navarro & Steinmetz 1997, 2000; van den Bosch, Burkert, & Swaters 2001). Spheroids, on the other hand, are thought to form either by a "monolithic collapse" (Eggen, Lyden-Bell, & Sandage 1962; Jimenez et al. 1999) or as a result of mergers of preexisting galaxies (Toomre 1977; Barnes & Hernquist 1992 and references therein). Detailed theoretical predictions for the statistical morphological properties of galaxies and their evolution have been calculated for the hierarchical merging formation mechanism appropriate to cold dark matter cosmologies (Kauffmann, White, & Guiderdoni 1993; Kauffmann 1995, 1996; Baugh, Cole, & Frenk 1996a, 1996b; Somerville, Primack, & Faber 2001). Among other things, these models give the relative luminosities and stellar masses of the spheroids and disks of galaxies.

In this work, we measure the *I*-band bulge-to-total light ratio (B/T) for a large sample of galaxies with spectroscopic redshifts by fitting two-dimensional models to the observed galaxy images. We use this information to estimate the spheroid and disk luminosity functions, as well as the total stellar mass that resides in disks and spheroids. An earlier attempt to estimate the relative contributions to the luminosity from spheroids and disks was carried out by Schechter & Dressler (1987), based on eyeball estimates of the B/T.

The remainder of this paper is arranged as follows. In § 2 we describe our basic data set. In § 3 we introduce the method used to fit model images to the data and thereby extract B/T (along with other interesting parameters) and describe how we estimate errors. In § 4 we examine the accuracy of our technique and determine how well the B/T can be measured as a function of the apparent magnitude of a galaxy. We then compute luminosity functions and total stellar masses for spheroids and disks. Finally, in § 5 we present our conclusions.

[1] California Institute of Technology, MC 105-24, Pasadena, CA 91125; abenson@astro.caltech.edu.
[2] Physics Department, University of Durham, Durham, DH1 3LE, England.

2. DATA

The galaxy sample used in this work is that of Gardner et al. (1997). The reader is referred to that work for a full description of the data. Here we summarize the most important features of the data set.

Imaging of two fields of total area 10 deg^2 was carried out in the B, V, and I bands using the T2KA camera on the Kitt Peak National Observatory (KPNO) 0.9 m telescope, resulting in images with $0\farcs68$ pixel^{-1}. Exposures of 300 s reached 5 σ detection depths of $B = 21.1$, $V = 20.9$, and $I = 19.6$ in $10''$ circular apertures. Imaging was also carried out in the K band using the IRIM camera on the KPNO 1.3 m telescope resulting in $1\farcs96$ per pixel images, and a 5 σ detection depth of $K = 15.6$ in a $10''$ circular aperture. The positions of the fields were chosen randomly (the field centers are R.A. 14^h15^m, decl. $+ 00^\circ$ and R.A. 18^h0^m, decl. $+ 66^\circ$). The I-band images, which we will use in this work, were bias-subtracted, flattened using twilight flats and with median sky flats. Objects were identified with the SEXTRACTOR program (Bertin & Arnouts 1996), using a 3 σ threshold. The seeing in the optical images varied in the range $1\farcs3 < \mathrm{FWHM} < 2\farcs0$. One field contained a nearby rich galaxy cluster.

Spectroscopic follow-up was obtained for a K-selected sample in subregions of total area 4.4 deg^2, using the Autofib-2 fiber positioner and WYFFOS spectrograph on the 4.2 m William Herschel Telescope on La Palma. Spectra were obtained for 567 galaxies with $K < 15$, which allowed redshifts to be measured for 510 galaxies (a redshift completeness of 90%). Although the spectroscopic sample is K-selected, this does not introduce any incompleteness in the $I < 16$ sample used extensively in this work (i.e., there are no galaxies with $I-K < 1$ in the sample). We also briefly consider an $I < 18$ sample, for which the spectroscopic completeness falls to around 50% because of the K-band selection (which also introduces a bias in this fainter sample against objects that are blue in $I-K$). For the $I < 16$ and $I < 18$ samples, the median redshift is $z = 0.08$ and 0.14, respectively.

3. METHOD

Wadadekar, Robbason, & Kembhavi (1999) have proposed a two-dimensional galaxy decomposition technique that can efficiently recover B/Ts (and other parameters) of model galaxy images with high accuracy (see also Byun & Freeman 1995; de Jong 1996). They present a detailed study of the effects of uncertainties in the point-spread function (PSF), the presence of nearby stars, and the stability of the B/T estimates as a function of the signal-to-noise ratio (S/N). Our approach is similar to theirs, but we apply the technique to a large photometric sample of real galaxies.[3] We consider the "real world" problems of automated masking of nearby galaxies and stars and make a thorough assessment of the errors in the measured parameters. We also present, in the Appendix, estimators for the luminosity functions of disks and spheroids.

For this analysis, we have used the sample of 636 $I < 18$ galaxies of Gardner et al. (1997) imaged in B, V, I, and K, as described in § 3. Postage stamp images of 33×33 pixels ($0\farcs68$ pixel^{-1}) around each galaxy were extracted from the I-band data. This was the best-observed band by Gardner et al. (1997) and is particularly well suited for our purposes because it minimizes the effects of young blue stars. This image size is large enough to include the entire region of the galaxy for which reasonable S/N is achieved (and in most cases extends well beyond it.) To determine the B/T, we fit the two-dimensional surface brightness profile of each galaxy using a combination of an exponential disk,

$$\Sigma_d(\theta) = \Sigma_{d,0} \exp(-\theta/\theta_d) \ , \tag{1}$$

and an $r^{1/4}$-law spheroid,

$$\Sigma_s(\theta) = \Sigma_{s,e} \exp\left\{-7.67\left[(\theta/\theta_e)^{1/4} - 1\right]\right\} \ , \tag{2}$$

where θ is the angular distance from the galaxy center. We will also consider a more general $r^{1/n}$ spheroid profile, as Wadadekar et al. (1999) did. The disk is allowed to be inclined and to have arbitrary position angle. The spheroid is allowed an ellipticity (defined as the ratio of semimajor to semiminor axes) in the range 1–6 and can also have an arbitrary position angle. To mimic seeing, we construct mock images using these profiles, which we then smooth with a Gaussian filter (integrated over each pixel to account for the variation of the PSF across the pixel),

$$p(\theta) = \exp\left[-(\theta/\sigma)^2/2\right]/2\pi\sigma^2 \ . \tag{3}$$

The width of the Gaussian is treated as a free parameter to account for variations in seeing between the images. (We examine in § 4.1 the effect of using a more realistic PSF.) The postage stamp images were centered on the galaxy of interest, but we allow the position of the image center to vary since in many cases the resulting subpixel variations lead to lower values of χ^2. We also allow a small contribution from a faint, constant surface brightness background in order to take into account small inaccuracies in sky subtraction. The best-fitting parameters for each galaxy were then obtained by minimizing χ^2 using Powell's algorithm (Brent 1973). There are a total of 12 fit parameters (13 if we include n when fitting $r^{1/n}$ spheroid profiles) summarized in Table 1.

TABLE 1

PARAMETERS USED TO CONSTRUCT MOCK GALAXY IMAGES IN THE FITTING PROCEDURE

Parameter	Definition
$\Sigma_{d,0}$	Disk central surface brightness
$\Sigma_{s,e}$	Spheroid surface brightness at the effective radius
θ_d	Disk angular scale length
θ_e	Spheroid effective radius
P_d	Disk position angle
P_s	Spheroid position angle
i	Disk inclination angle
e	Spheroid ellipticity
(x, y)	Center of image
B	Excess background surface brightness
σ	Seeing[a]
n	Spheroid profile index[b]

[a] See eq. (3).

[b] Fixed at $n = 4$ unless otherwise stated.

[3] Wadadekar et al. (1999) applied their technique to three galaxies for which previous estimates of B/T were available and found reasonable agreement.

In § 4.1 we will consider how accurately this procedure recovers the B/T of the galaxies.

A significant fraction of the postage stamp images was contaminated by a secondary galaxy (and occasionally by more than one). We use a simple algorithm to identify such contaminants and mask them from the image. The aim is to remove objects that are physically distinct from the galaxy of interest without masking any pixels of the galaxy itself. We first rank the pixels in the image by surface brightness and then proceed to find groups of bright pixels. The brightest pixel is assigned to the first group. Successive pixels are assigned to a preexisting group if they touch it (i.e., if they are adjacent either horizontally, vertically or diagonally) or else are assigned to a new group. In the case where a pixel touches more than one group, the two groups are merged. This process is continued until pixels of a fixed S/N are reached (specifically, we consider only pixels more than 3 σ above the sky background). If more than one group exists at this point, the group at the center is deemed to be the galaxy of interest, and the pixels of all secondary groups are marked as being contaminated and are not included in the χ^2 sum. This simple algorithm works well in the majority of cases, but it fails in a few (28 out of 636 galaxies), either by not removing a contaminating galaxy or by removing a significant fraction of the primary galaxy. Rather than attempting to use a more complex algorithm in these cases, we resorted to cleaning the image by hand (i.e., we view the image and manually mark the contaminated pixels).

The majority of galaxies (363 out of 626) are fitted reasonably well by this procedure. We regard a galaxy as being reasonably well fitted when Q, the probability that the measured value of χ^2 is exceeded by random fluctuations, is greater than 5%. Not surprisingly, however, many galaxies are not well fitted. These typically show signs of strong morphological disturbance (perhaps because of a recent or imminent merger) or other inhomogeneities. Examples of well-fitted and poorly fitted galaxies are given in Figure 1. Poorly fitted galaxies are easily identified by their large χ^2 values and so may be excluded from further analysis if desired. It should be noted that a poor fit does not indicate a failure of our fitting procedure per se, rather it signals that the galaxy is not well described by a combination of a spheroid and a disk. We choose to show results computed using the entire sample, regardless of how well a galaxy was fitted, but we will comment on how our results change if badly fitted galaxies are excluded from the analysis.

Errors on the fitted parameters could, in principle, be determined using a $\Delta\chi^2$ approach, but this would require mapping χ^2 in the 12 dimensional parameter space of the fit—an exceedingly time consuming exercise—and, in any case, the errors are unlikely to be normally distributed given that the model is highly nonlinear in the parameters. We therefore adopt a Monte Carlo approach to error estimation. Using the best-fitting model for each galaxy, we generate 30 realizations of that model, add random noise at the same level as in the real image, and mask out any pixels that were masked out in the original. We then find the best-fitting parameters for each realization and take their distribution as indicative of the uncertainties in the actual fit. It should be noted that this is only a valid procedure if the original image is well fitted by the model. In procedures where this is not the case, there is no reason to expect the Monte Carlo distributions to give an estimate of the true errors. The B/T distributions for the three galaxies illustrated in Figure 1 are shown in that figure.

4. RESULTS

4.1. *Accuracy Checks*

We begin by assessing the reliability of our procedure for recovering the true B/T of a galaxy (assuming, of course, that real galaxies are well described by our model). Our Monte Carlo procedure for error estimation allows a determination of the accuracy of our technique. For each galaxy, the value of B/T input into the Monte Carlo simulations may be compared to the mean and standard deviation of the distribution of 30 recovered B/T values. Figure 2 gives the results of these accuracy tests. The left-hand panel shows the standard deviation of the recovered B/T as a function of the I-band apparent magnitude of the mock image. For bright galaxies ($m_I \lesssim 16$), $\sigma_{\rm MC}$ is fairly small, typically less than about 0.1. However, for fainter galaxies, $\sigma_{\rm MC}$ increases very rapidly, resulting in rather poorly constrained B/T values. (In reality, $\sigma_{\rm MC}$ depends also upon the other parameters that describe the mock image, but the correlation with apparent magnitude is the most important.)

In the right-hand panel of Figure 2, we plot the mean value of B/T recovered from the Monte Carlo simulations against the true value for the mock image. The large solid circles indicate those images for which $\sigma_{\rm MC} \leq 0.1$. Evidently, for these galaxies, the value of B/T is recovered accurately and without any strong systematic bias. The small dots show the results for all other galaxies. Now the scatter is much larger, and, more importantly, there are systematic biases in the mean recovered B/T, such that very low and very high values are avoided. This effect is not surprising; the values of B/T for these faint galaxies are almost entirely unconstrained. (Note that the standard deviation for a completely uniform distribution of B/T is approximately 0.3.) As a result, the distribution of B/T from the Monte Carlo simulations becomes close to uniform, with the mean tending toward 0.5 as $\sigma_{\rm MC}$ increases. For the 90 galaxies in our sample with $m_I \leq 16$, there is a tight correlation between $(\mathrm{B/T})_{\rm true}$ and the mean value recovered from the Monte Carlo simulations, and it is this subsample that we will use below to compute luminosity functions. Unfortunately, its relatively small size limits the statistical accuracy of our estimates quite considerably.

To find the best-fit solution we must choose initial values for the parameters to be fitted and then use Powell's algorithm to search for values producing a better fit. For parameters such as the position angles, disk inclination, and spheroid/disk sizes, we make initial guesses based on the image being fitted. Other parameters are initially assigned "typical" values. We have checked the effect of altering these initial values. For galaxies with $\sigma_{\rm MC} \leq 0.1$, the choice of initial value makes almost no difference to the recovered values of the parameters, indicating that our technique is finding the true minimum χ^2. As $\sigma_{\rm MC}$ becomes larger, however, the recovered parameters begin to depend strongly upon the initial values chosen. For these images, the χ^2 surface in the 12 dimensional parameter space does not possess an obvious minimum (i.e., it is very noisy). This is just another way of saying that the values of the fitted parameters for these faint images are highly uncertain.

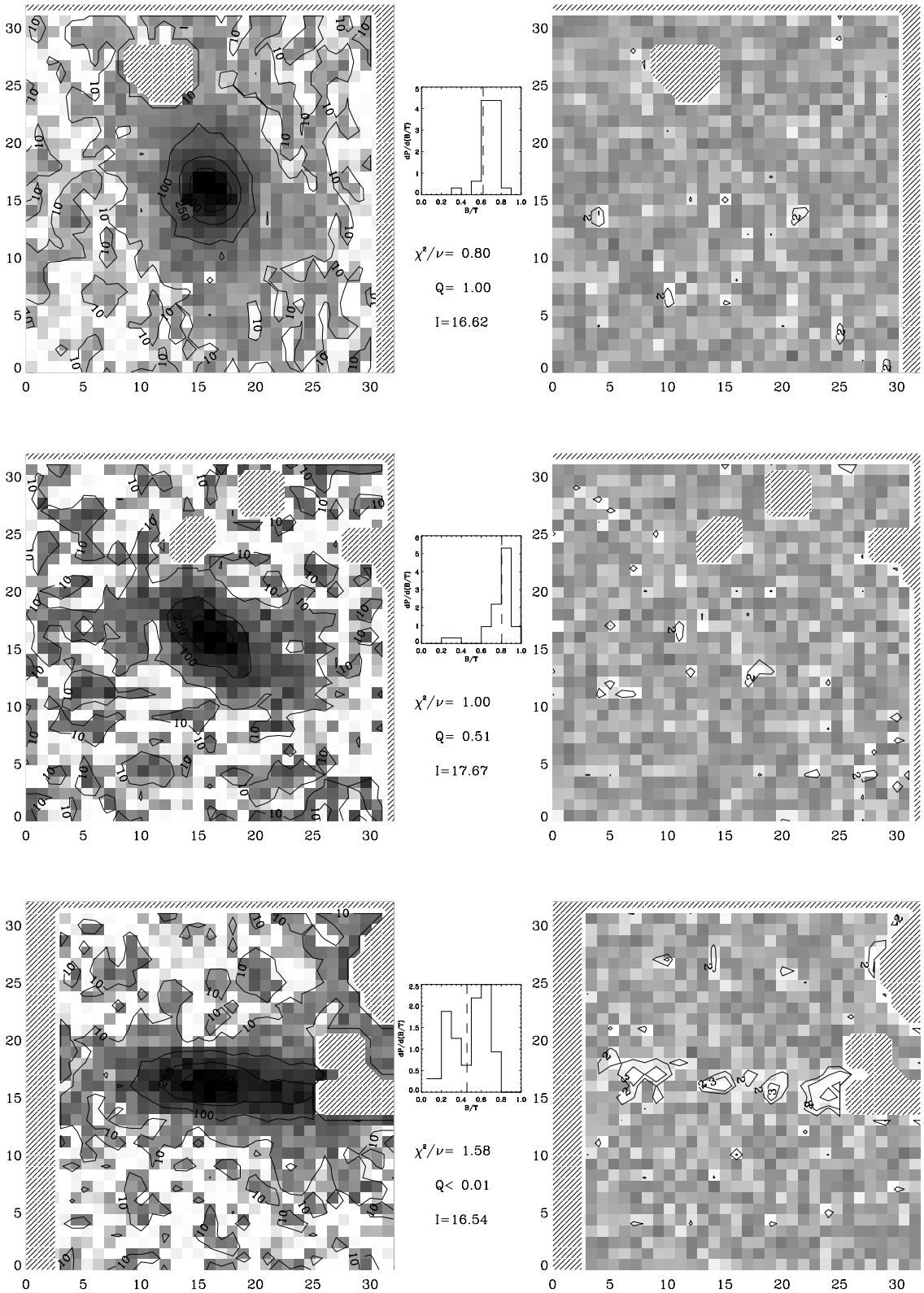

FIG. 1.—Postage stamp images of three representative galaxies from our sample. The top row shows a galaxy that is fitted very well by our procedure, the bottom row shows one that is poorly fitted, and the middle row shows a more typical result. The left-hand column is the original 33×33 pixel galaxy image with contours indicating the pixel value in ADUs. The right-hand column is the residual image after subtracting the best-fit model galaxy. Contours show the absolute value of the residual in units of σ, the rms uncertainty on each pixel value. Hatched regions contained contaminant galaxies and were removed by our automated cleaning procedure before fitting. (Where an entire row or column is hatched, the postage stamp image was recentered prior to fitting.) Between the original image and the residual maps we quote the value of χ^2 per degree of freedom Q (the probability that a random fluctuation exceeds this value of χ^2) and the I-band apparent magnitude. Also shown is a histogram of dP/d (B/T), the distribution of bulge-to-total light ratios found from the Monte Carlo simulations described in the text, with a vertical dashed line indicating the best-fit B/T value for the original image.

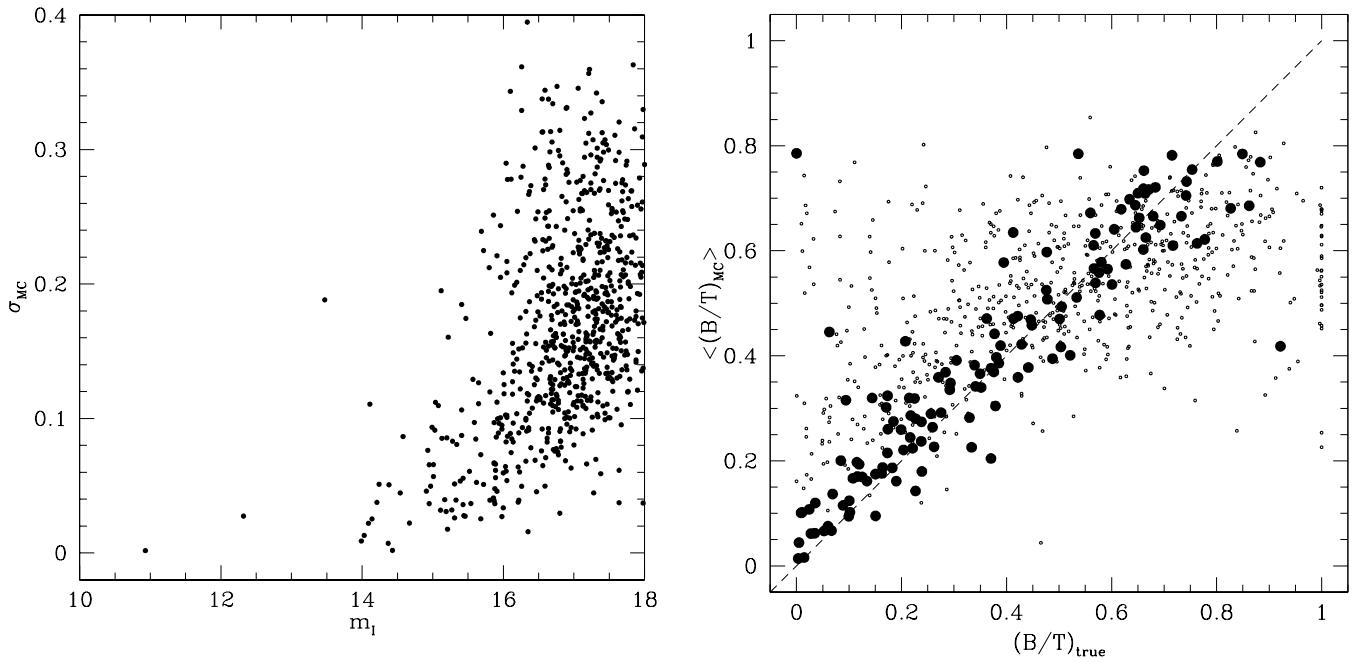

FIG. 2.—*Left:* Standard deviation, σ_{MC}, of the distribution of recovered B/Ts from 30 Monte Carlo realizations of a model galaxy image, as a function of the apparent *I*-band magnitude of the model image. *Right:* Mean recovered B/T from 30 Monte Carlo realizations of a model galaxy image plotted against the true B/T value. Large filled circles show those galaxies for which $\sigma_{MC} \leq 0.1$, while small open circles show all other galaxies.

Andredakis, Peletier, & Balcells (1995) have demonstrated that the bulges of spiral galaxies are more accurately fitted by an $r^{1/n}$, rather than by the more usual $r^{1/4}$, surface brightness profile, with values of n ranging from around 1 to 6 (similar variations in n are seen for elliptical galaxies; Bingelli & Cameron 1991; Caon, Capaccioli, & D'Onofrio 1993). They show that the value of n is strongly correlated with morphological type. Although our present data provide only rather poor constraints on the value of n (owing to limited angular resolution and S/N), we have nevertheless repeated the fitting procedure using $r^{1/n}$ profiles for the spheroids, treating n as a free parameter. For galaxies where the B/T is well determined, we find that there is a strong correlation between the B/T values obtained with $r^{1/4}$ and $r^{1/n}$ profiles, although inevitably some scatter is present. The disk and spheroid luminosity functions computed using B/Ts from $r^{1/n}$ fits show no statistically significant difference from those using $r^{1/4}$ fits.

Finally, we remind the reader that our analysis makes use of a Gaussian PSF to mimic the effects of seeing in the data. A Gaussian accurately describes the core of the PSF measured from bright stars in the images. However, a profile consisting of a Gaussian core plus power-law wings provides a better match to many of the stellar profiles. (The variation of Gaussian and core components from night to night in the imaging data is not so well characterized, however, and this is why we make use of a simple Gaussian for our main analysis.) Fitting the images using such a profile (keeping the relative proportions of Gaussian and power-law wings fixed, but allowing the overall radial scale of the PSF to be a free parameter) results in small changes in the B/T, typically significantly smaller than the error in the best-fit value. Thus, the luminosity functions presented below are unaffected by the exact choice of PSF. However, it is clear that a good characterization of the PSF and its variation will be crucial to obtain accurate disk and spheroid luminosity functions from larger, higher quality data sets.

4.2. *Luminosity Functions*

Using the $I < 16$ sample of approximately 90 galaxies for which we have good estimates of the B/T, we now proceed to estimate the disk and spheroid luminosity functions. Our aim here is to develop the techniques required for this measurement and demonstrate them using a particular data set. Given the small size of the data set, we must expect that both statistical (due to the small number of galaxies) and systematic (due, for example, to the lack of rich clusters in the data set) errors will be present. These issues are considered further in § 5.

To determine the present-day luminosity functions, we need to apply $k + e$ corrections to the galaxy luminosities. We use the type-dependent $k + e$ corrections obtained by Gardner et al. (1997). Briefly, a set of model galaxy colors was computed using an updated version of the Bruzual & Charlot (1993) stellar population models with a range of star formation histories. The observed colors of each galaxy were matched to one of the models, and that particular model was then used to extrapolate the observed galaxy luminosity to $z = 0$. Note that our type-dependent $k + e$ corrections are based on the *total* (i.e., disk plus spheroid) color of each galaxy. In principle, $k + e$ corrections could be applied to each component separately if spheroid/disk decompositions were carried out in several bands. Given the uncertainties in our present estimates of B/T, we refrain from this degree of complexity in this analysis.

We use the stepwise maximum likelihood (SWML) estimator proposed by Efstathiou, Ellis, & Peterson (1988, hereafter EEP88) and also the parametric maximum likelihood method proposed by Sandage, Tammann, & Yahil

(1979, hereafter STY79) to compute disk and spheroid luminosity functions. The detectability of a spheroid depends on both its apparent magnitude and the B/T, and we must account for this in constructing the likelihood function. This leads us to define a two-dimensional function, $\Phi(M,\ B)$, such that $\Phi(M,\ B)dM\,dB$ is the number of galaxies per unit volume with B/T in the range B to $B + dB$ and *spheroid* absolute magnitude in the range M to $M + dM$ (with an equivalent definition for disks). The application of the maximum likelihood estimator to this function is discussed in detail in the Appendix. The normal luminosity function of spheroids is readily derived using $\phi(M) = \int_0^1 \Phi(M,\ B)dB$ (and similarly for disks). For the STY79 method we must assume some parametric form for the luminosity function. We have tried fitting the disk and spheroid luminosity functions with a "Schechter × exponential" form, namely, $\Phi(M,\ B) = \phi(M)\exp(\beta B)$, where $\phi(M)$ is the normal Schechter function and β is a parameter to be fitted, motivated by the shape of the SWML estimate of these luminosity functions.

Figure 3 shows the resulting *I*-band luminosity functions with distances computed assuming $(\Omega_0,\ \Lambda_0) = (0.3,\ 0.7)$[4] and $H_0 = 100\ h$ km s^{-1} Mpc^{-1}. Triangles show the total luminosity function; circles and stars show the spheroid and disk luminosity functions separately. These SWML luminosity functions are normalized to the *I*-band number counts in the Sloan Digital Sky Survey (SDSS) using the procedure described in the Appendix. For the total luminosity function, we plot the standard SWML error bars (obtained from the covariance matrix of the luminosity function as described by EEP88), but for the spheroid and disk luminosity functions, the error bars are the sum in quadrature of the standard SWML errors and the variance in the luminosity function estimated from the 30 Monte Carlo realizations of the spheroid/disk decomposition process. The errors from each source are of comparable magnitude (although the variance from the Monte Carlo realizations is the smaller of the two). The very thick solid line shows the best-fitting Schechter function to the total luminosity function (determined using the STY79 method); the inset shows the values of α and M_* for this fit, together with their 1 and 2 σ error contours. (The small sample size is reflected in rather large and correlated uncertainties in M_* and α.) Thick and thin solid lines show the best-fit STY79 Schechter × exponential luminosity function fits to the spheroid and disk luminosity functions, respectively (with the corresponding confidence ellipses for α and M_* shown in the inset, and the values of β given in the figure caption). A likelihood ratio test (EEP88) shows that the Schechter × exponential luminosity function is not a particularly good fit to the data. With the present small data set we have been unable to find a better functional form. This situation will be rectified with a larger data set (assuming that some suitable functional form does actually exist).

[4] Assuming $(\Omega_0,\ \Lambda_0) = (1,\ 0)$ instead changes our results only slightly, shifting the luminosity function faintward because of the smaller luminosity distance in this model.

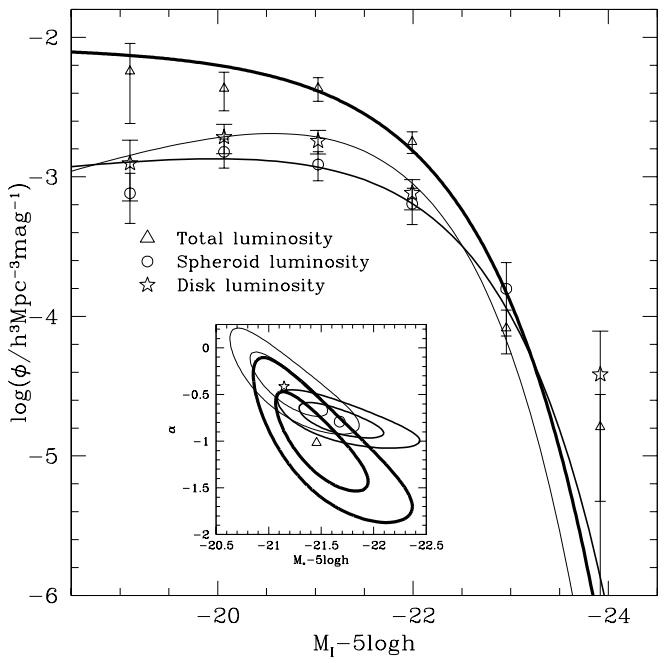

FIG. 3.—*I*-band luminosity functions. Triangles, circles, and stars show the SWML estimates of the total, spheroid, and disk luminosity functions, respectively. Only galaxies brighter than $I = 16$ have been used, $k + e$ corrections have been applied to all galaxies, and distances have been calculated assuming $(\Omega_0,\ \Lambda_0) = (0.3,\ 0.7)$. Error bars are the sum in quadrature of the standard SWML errors and the variance in estimates of the luminosity function from 30 Monte Carlo realizations of the spheroid/disk decomposition procedure. The very thick solid line shows the best-fit Schechter function to the total luminosity function, while the inset shows the values of α and M_* for this fit, together with their 1 and 2 σ error ellipses. Thick and thin solid lines show the best-fit Schechter × exponential functions to the spheroid and disk luminosity functions, respectively, and confidence regions for α and M_* for these fits are given in the inset (the remaining parameter of the fits was $\beta = 0.0 \pm 0.37$ and 2.1 ± 0.37 for spheroids and disks, respectively).

The *I*-band luminosity functions of disks and spheroids are remarkably similar. The only significant difference is that the spheroid luminosity function is somewhat lower at faint magnitudes. However, given the small size of the present sample, this difference may not be robust. The luminosity densities in disks and spheroids obtained by integrating the SWML luminosity functions over the range of absolute magnitudes shown in Figure 3 are 5.8 ± 0.8 and $4.7 \pm 0.7 \times 10^7\ h\ L_\odot$ Mpc^{-3}, respectively (where we have taken $M_\odot = 4.14$ in the *I* band; Cox 2000). In principle, we can use our Schechter × exponential fits to estimate the total luminosity density, extrapolating to include the contribution from arbitrarily faint spheroids and disks. Doing so yields results that agree with the SWML estimates within the quoted errors, suggesting that our determination may have suitably converged. However, it must be kept in mind that the Schechter × exponential form is not a particularly good fit to the current data sets.

In Figure 4, we show slices through the bivariate luminosity function, $\Phi(M,\ B)$, at constant M for several values of M (as indicated in the figure, and in bins of width $\Delta M = 0.48$). It is evident that $\Phi(M,\ B)$ is *not* independent of B and that, in fact, it may not be separable into a simpler form $\Phi(M,\ B) = \phi(M)g(B)$. This is particularly noticeable for the spheroid luminosity function. Figure 4 shows that spheroid-dominated systems (i.e., B/T > 2/3) are found only in the brightest spheroids, while disk-dominated systems (i.e., D/T > 2/3) have disks with a much broader range of luminosities. This point is made more clearly in Figure 5, where we show the spheroid luminosity function of spheroid-dominated systems and the disk luminosity function of disk-dominated systems. We find spheroid-dominated systems in abundance only brightward of

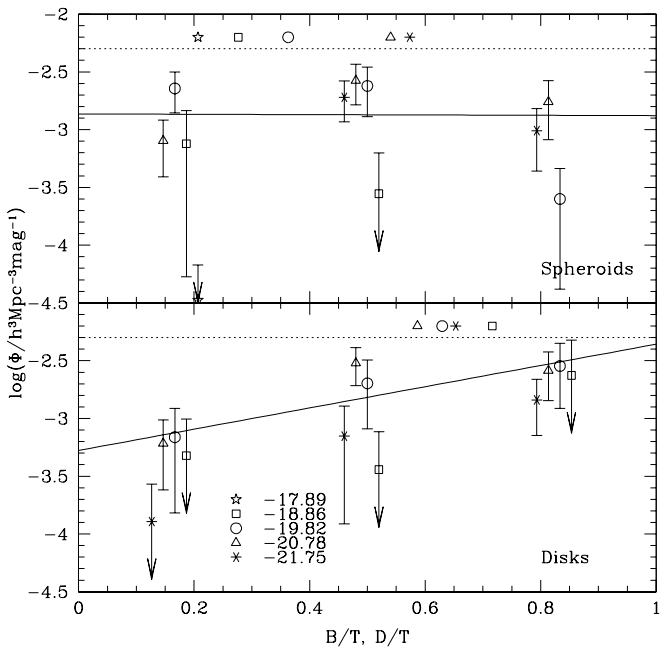

FIG. 4.—Slices through the SWML estimate of the bivariate luminosity function, $\Phi(M,\ B)$, for different absolute magnitudes, M, as indicated in the figure. Points were computed in bins of size $(\Delta M,\ \Delta B) = (0.48,\ 0.33)$ and errors obtained as described by EEP88. The upper panel shows the spheroid luminosity function, and the lower panel the disk luminosity function. The points without error bars above the dotted line in each panel indicate the mean B/T (and D/T) for spheroids (and disks) in the corresponding absolute magnitude bins. Solid lines indicate the best-fit Schechter × exponential parametric luminosity function for the $M_I - 5\log h = -19.82$ bin.

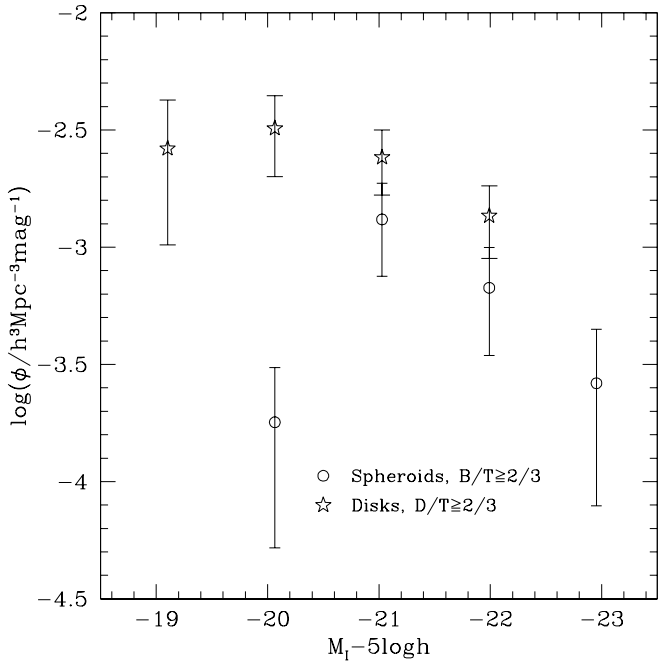

FIG. 5.—SWML estimates of the I-band luminosity functions of spheroids in spheroid-dominated galaxies (i.e., $B/T > 2/3$; *circles*) and disks in disk-dominated galaxies (i.e., $D/T > 2/3$; *stars*). The samples include 13 and 36 galaxies, respectively. Errors are the sum in quadrature of the standard SWML errors and the variance found in luminosity functions estimated from 30 Monte Carlo realizations of the spheroid/disk decomposition procedure.

$M_I - 5\log h \approx -21$ but disk-dominated systems across the whole range of luminosities.

4.3. *The Stellar Mass in Disks and Spheroids*

The stellar mass associated with the luminosity of each galaxy is easily obtained by a similar procedure to that employed to calculate the k-corrections (namely, fitting their *BVIK* colors to a set of template galaxies). We use these estimates to construct the stellar mass functions of spheroids and disks in the local universe and thereby estimate the total mass content in each component. The method that we adopt is the same that Cole et al. (2001) used to measure the *total* stellar mass density in the universe from a combination of Two-Degree Field Galaxy Redshift Survey and Two Micron All Sky Survey data. Cole et al. (2001) found the stellar mass density[5] in units of the critical density to be $\Omega_{\rm stars} = 0.0016 \pm 0.00024\ h^{-1}$ or $\Omega_{\rm stars} = 0.0029 \pm 0.00043\ h^{-1}$, depending on whether a Kennicutt (1983) or a Salpeter (1955) stellar initial mass function (IMF) was assumed. (Both estimates include the effects of dust on galaxy luminosities as described by Cole et al. 2001.) We normalize our stellar mass functions by requiring them to produce the same number density of galaxies more massive than M_* as the Cole et al. (2001) stellar mass function. The total stellar mass density inferred from our $I < 18$ sample is then $\Omega_{\rm stars} = 0.0009 \pm 0.00007\ h^{-1}$ or $\Omega_{\rm stars} = 0.0017 \pm 0.00012\ h^{-1}$ for the same two IMFs, respectively, and the same prescription for dust-extinction. Errors on the stellar mass density were found by summing in quadrature the error from each individual bin in the SWML mass function, together with the error in the overall normalization. Our estimates include contributions from galaxies with stellar masses greater than $10^9\ h^{-2}\ M_\odot$ below which the SWML stellar mass function is not well determined. We can check our result using the STY79 stellar mass function. For this, we fit a Schechter function convolved with a Gaussian of width 0.1 in $\log_{10} M_{\rm stars}$ to account for the scatter in the relation between stellar mass and I-band absolute magnitude. We find that our estimates of $\Omega_{\rm stars}$ using the SWML and STY79 mass functions agree within the errors, suggesting that the result has already converged to sufficient accuracy. Our estimates, however, are lower than those of Cole et al. (2001), a reflection of the flatter faint end slope of our mass functions that may well be due to the small size of our sample.

For our $I < 16$ sample, for which the B/T is well measured, we find a slightly higher total stellar mass density of $\Omega_{\rm stars} = 0.0012 \pm 0.00014\ h^{-1}$ for the Kennicutt (1983) IMF. Splitting into spheroidal and disk components, we find

$$\Omega_{\rm stars,\,spheroids} = 0.00039 \pm 0.00006\ h^{-1}$$

and

$$\Omega_{\rm stars,\,disks} = 0.00051 \pm 0.00008\ h^{-1}\ ,$$

[5] Specifically, Cole et al. (2001) estimated the mass locked up in stars and stellar remnants, which differs from the time integral of the star formation rate due to recycling of material by massive stars. We adopt the same definition of stellar mass here.

for this same IMF. (Note that with the SWML method the stellar mass densities of disks and spheroids are not guaranteed to sum to give the total stellar mass density.) If, instead, we assume a Salpeter IMF, the ratio of disk to spheroid stellar mass densities increases slightly from 1.31 to 1.37, but this change is negligible given the current errors in these quantities. Although the small size of our sample is clearly a significant limitation, this initial result suggests that spheroids and disks contribute about equally to the stellar mass density of the universe. The techniques developed in this paper, when applied to a much larger data set, should allow their contributions to be more accurately determined.

5. DISCUSSION

We have presented a detailed method to determine the bulge-to-total light ratios of galaxies by fitting to two-dimensional photometry and have applied this technique to determine the *I*-band bulge-to-total luminosity ratios of a sample of approximately 600 galaxies brighter than $I = 18$ with spectroscopic redshifts. Our approach is designed to work with realistic galaxy images, dealing automatically with contamination by nearby objects, a varying PSF, and small changes in the background from image to image. A crucial part of the fitting procedure is a Monte Carlo determination of the errors on the fitted parameters, an approach that is favored since it is fast and automatically accounts for the highly nonlinear nature of the model parameters. For the current sample of galaxies, around 60% are well fitted by a combination of an exponential disk and an $r^{1/4}$-law spheroid. Those that are not well fitted frequently show signs of morphological disturbance. We find that bulge-to-total light ratios are determined accurately (i.e., with errors of around 10%) only for galaxies brighter than $I \approx 16$.

For the 90 galaxies brighter than $I = 16$ in this sample we measure the B/T with reasonable accuracy. We have used the resulting disk/spheroid decomposition of these bright galaxies to construct separate luminosity functions for disks and spheroids. We find no significant differences between them when considered purely in terms of luminosity, although the statistical uncertainties associated with the small sample size make the detection of any differences difficult. However, when we consider the bivariate distributions of luminosity and bulge-to-total or disk-to-total light, we find that spheroid-dominated systems ($B/T > 2/3$) only occur for the brightest spheroids, while disk-dominated systems ($D/T > 2/3$) occur for a much broader range of disk luminosities.

The relative contributions of disks and spheroids to the total stellar mass density in the universe is a very important constraint on theories of galaxy formation that attempt to describe the assembly of galaxies as a function of time. We find, perhaps surprisingly, that the disks and spheroids in our sample contribute almost equally to the stellar mass density today (in a ratio of 1.3 ± 0.2). Since the stellar populations in disks are generally younger than those in spheroids, it is an interesting coincidence that the total stellar mass in the two kinds of structural components should be so similar at the present time.

Schechter & Dressler (1987) reached a similar conclusion to ours using a photometric comparison technique to estimate the *B*-band bulge-to-disk ratios of galaxies. While this technique may not be as accurate as our own on a galaxy-by-galaxy basis, it should provide a good estimate of the total contribution of each component to the stellar mass density. It is therefore reassuring that our results agree well with those of Schechter & Dressler (1987). A different result was obtained by Fukugita, Hogan, & Peebles (1998), who derived a ratio of disk to spheroid stellar mass density of 0.33 ± 0.23. Although they found comparable *B*-band luminosity density in spheroids and disks, they adopted a spheroid mass-to-light ratio around 4 times greater than that for disks, resulting in spheroids making a significantly greater contribution to the stellar mass density. While we use a more accurate technique for converting from luminosity to stellar mass (a technique that could be improved further if B/Ts were measured for each galaxy in several bands), the small size of our sample limits the accuracy of our results. In particular, our sample may not contain enough rich clusters that are known to contain higher fractions of spheroid-dominated galaxies than the field (e.g., Dressler 1980), and this could introduce a small bias in our results.

Clearly the greatest limitation of this work is the small size of the sample of galaxies for which accurate disk/spheroid decompositions can be performed. Fortunately, this problem should be remedied in the near future with the advent of high-quality, large-area photometric surveys, such as that being carried out by the SDSS project.

We thank Jon Gardner and Carlton Baugh for supplying data used in this work and for valuable discussions, and the referee, Alan Dressler, for valuable suggestions. We also thank Istvan Szapudi for his assistance in the early stages of this work.

APPENDIX

ESTIMATORS FOR SPHEROID AND DISK LUMINOSITY FUNCTIONS

The traditional $1/V_{\max}$ estimator is trivially adapted to the case of disk and spheroid luminosity functions. The estimator is applied just as in the case of the standard luminosity function, except that the *total* luminosity of the galaxy (i.e., disk plus spheroid luminosity) is used to compute $V_{\max}$, since it is this total luminosity that determines the volume within which the galaxy could have been detected.

The maximum likelihood estimator of EEP88 is also easily generalized to the case of spheroid and disk luminosity functions. Consider the case of the spheroid luminosity function (the same arguments apply to disks). As noted earlier, the detectability of a spheroid depends upon both its absolute magnitude, *M*, and on the bulge-to-total light ratio which we denote by *B* in this Appendix. We begin, therefore, by defining a two-dimensional function, $\Phi(M,\ B)$, such that $\Phi(M,\ B)dM\,dB$ is the number of galaxies with bulge-to-total light ratio in the range *B* to $B + dB$ and *spheroid* absolute magnitude *M* to $M + dM$ per unit volume. The normal luminosity function of spheroids is easily recovered using $\phi(M) = \int_0^1 \Phi(M,\ B)dB$. The probability that

galaxy i with spheroid magnitude M_i and bulge-to-total light ratio B_i is seen in a magnitude limited survey is

$$p_i \propto \Phi(M_i,\ B_i) \int_0^1 \int_{-\infty}^{M'_{\rm lim}(z_i,B)} \Phi(M,\ B) dM\, dB\ , \tag{A1}$$

where $M'_{\rm lim}(z_i,\ B) = M_{\rm lim}(z_i) - 2.5\log_{10} B$ and $M_{\rm lim}(z_i)$ is the limiting absolute magnitude of the survey at redshift z_i. The use of $M'_{\rm lim}$ is necessary since arbitrarily faint spheroids will make it into the survey provided that they have a sufficiently low bulge-to-total light ratio (corresponding to sufficiently bright disks).

From this definition we can construct the usual likelihood function

$$\ln \mathscr{L} = \sum_{i=1}^{N} \ln \Phi(M_i,\ B_i) - \sum_{i=1}^{N} \ln \left[\int_0^1 \int_{-\infty}^{M'_{\rm lim}(z_i,B)} \Phi(M,\ B) dM\, dB \right] + {\rm const}\ , \tag{A2}$$

where N is the total number of galaxies. There are now two ways to proceed. In the first we assume a simple parametric form for $\Phi(M,\ B)$ and maximize the likelihood with respect to the parameters. This is analogous to fitting a Schechter function (Schechter 1976) to the normal luminosity function (e.g., Sandage, Tammann, & Yahil 1979). A simple parametric form that we have tried to fit to our data is

$$\Phi(M,\ B) = \phi(M) \exp(\beta B)\ , \tag{A3}$$

where $\phi(M)$ is the usual Schechter function and β is a parameter to be estimated from the fit. With this method, the likelihood function of equation (A2) can be evaluated for each value of the three parameters α, β, and M_*, and hence the parameter values that maximize the likelihood are readily obtained.

The second approach involves splitting $\Phi(M,\ B)$ into bins in M and B and treating each as a parameter. This is equivalent to the SWML method of EEP88 for estimating the standard luminosity function.

We represent $\Phi(M,\ B)$ as follows:

$$\Phi(M,\ B) = \Phi_{k,h} \begin{cases} M_k - \Delta M/2 < M < M_k + \Delta M/2, & k = 1, \ldots, N_p\ , \\ B_h - \Delta B/2 < B < B_h + \Delta B/2, & h = 1, \ldots, N_q\ , \end{cases} \tag{A4}$$

The likelihood function may then be written as

$$\ln \mathscr{L} = \sum_{i=1}^{N} W(M_i - M_k,\ B_i - B_h) \ln \Phi_{k,h} - \sum_{i=1}^{N} \ln \left\{ \sum_{h=1}^{N_q} \sum_{k=1}^{N_p} \Phi_{k,h} \Delta M \Delta B H[M_k,\ B_h,\ M_{\rm lim}(z_i)] \right\} + {\rm const}\ , \tag{A5}$$

where

$$W_{k,h}(M_i,\ B_i) = \begin{cases} 1 & \text{if } M_k - \Delta M/2 < M_i < M_k + \Delta M/2 \text{ and} B_h - \Delta B/2 < B_i < B_h + \Delta B/2 \\ 0 & \text{otherwise} \end{cases} \tag{A6}$$

and

$$H[M_k, B_h, M_{\rm lim}(z_i)] = \frac{1}{\Delta M \Delta B} \int_{B_h - \Delta B/2}^{B_h + \Delta B/2} \int_{M_k - \Delta M/2}^{M_k + \Delta M/2} Q(M,\ B) dM\, dB\ , \tag{A7}$$

where $Q(M,\ B) = 0$ if $M > M_{\rm lim}(z_i) - 2.5\log_{10} B$ and $Q(M,\ B) = 1$ otherwise. Since only the shape of the luminosity function is constrained by the above likelihood function, we introduce an additional constraint, $g = \sum_k \sum_h \Phi_{k,h} (L_{k,h}/L_f)^{\beta} \Delta M \Delta B - 1 = 0$, where $L_{k,h}$ is the total luminosity of a galaxy with spheroid magnitude M_k and bulge-to-total light ratio B_h and L_f is a fiducial luminosity (which we will take to be that corresponding to $M_I - 5\log h = -20.5$), using a Lagrangian multiplier λ as did EEP88. Maximizing $\ln \mathscr{L}' = \ln \mathscr{L} + \lambda g$ then yields

$$\Phi_{k,h} = \frac{\sum_{i=1}^{N} W(M_i - M_k,\ B_i - B_k)}{\sum_{i=1}^{N} H[M_k, B_h, M_{\rm lim}(z_i)] / \sum_{l=1}^{N_p} \sum_{m=1}^{N_q} \Phi_{l,m} H[M_l, B_m, M_{\rm lim}(z_i)]}\ , \tag{A8}$$

which are easily solved with an iterative procedure. The covariance matrix for the parameters is obtained in a manner entirely analogous to that outlined by EEP88.

Normalization of the maximum likelihood luminosity function can be achieved using the actual redshift data as described by Loveday et al. (1992) but using $M'_{\rm lim}$ in the selection function to account for the effects of the bulge-to-total light ratio. A better approach is to normalize by performing a least-squares fit to the number counts of galaxies from a wide area survey. The cumulative number count to apparent magnitude m is given by

$$n(m) = \int_0^{\infty} \int_0^1 \int_{-\infty}^{M'_{\rm lim}} \Phi[m - D(z) - K(z) - 2.5\log_{10} B,\ B] \frac{dV}{dz} dM\, dB\, dz\ , \tag{A9}$$

where $D(z)$ and $K(z)$ are the distance modulus and $k + e$ correction, respectively, at redshift z, which we can compute from the SWML estimate of Φ.

REFERENCES

Abraham, R. G., van den Bergh, S., Glazebrook, K., Ellis, R. S., Santiago, B. X., Surma, P., & Griffiths, R. E. 1996, ApJS, 107, 1
Andredakis, Y. C., Peletier, R. F., & Balells, M. 1995, MNRAS, 275, 874
Barnes, J. E., & Hernquist, L. 1992, ARA&A, 30, 705
Baugh, C. M., Cole, S., & Frenk, C. S. 1996a, MNRAS, 282, L27
———. 1996b, MNRAS, 283, 1361
Bertin, E., & Arnouts, S. 1996, A&AS, 117, 393
Bingelli, B., & Cameron, L. M. 1991, A&A, 252, 27
Brent, R. P. 1973, Algorithms for Minimization without Derivatives (Englewood Cliffs: Prentice Hall), chap. 7
Bruzual, G., & Charlot, S. 1993, ApJ, 405, 538
Byun, Y. I., & Freeman, K. C. 1995, ApJ, 448, 563
Caon, N., Capaccioli, M., & D'Onofrio, M. 1993, MNRAS, 265, 1013
Cole, S., et al. 2001, MNRAS, 326, 255
Cox, A. N. 2000, Allen's Astrophysical Quantities (4th ed.; New York: AIP)
de Jong, R. S. 1996, A&AS, 118, 557
de Vaucouleurs, G. 1959, Hand. Physik, 53, 275
Dressler, A. 1980, ApJ, 236, 351
Efstathiou, G., Ellis, R. S., & Peterson, B. A. 1988, MNRAS, 232, 431 (EEP88)
Eggen, O. J., Lynden-Bell, D., & Sandage, A. R. 1962, ApJ, 136, 748
Fukugita, M., Hogan, C. J., & Peebles, P. J. E. 1998, ApJ, 503, 518
Gardner, J. P., Sharples, R. M., Frenk, C. S., & Carrasco, B. E. 1997, ApJ, 480, L99
Hoyle, F. 1949, in Problems of Cosmical Aerodynamics, ed. J. M. Burgers & H. C. van de Hulst (Dayton: Central Air Documents Office), 195
Hubble, E. 1926, ApJ, 64, 321
Jimenez, R., Friaca, A. C. S., Dunlop, J. S., Terlevich, R. J., Peacock, J. A., & Nolan, L. A. 1999, MNRAS, 305, L16
Kauffmann, G. 1995, MNRAS, 274, 161
———. 1996, MNRAS, 281, 487
Kauffmann, G., White, S. D. M., & Guiderdoni, B. 1993, MNRAS, 264, 201
Kennicutt, R. C. 1983, ApJ, 272, 54
Loveday, J., Peterson, B. A., Efstathiou, G., & Maddox, S. J. 1992, ApJ, 390, 338
Naim, A., et al. 1995, MNRAS, 274, 1107
Navarro, J. F., Frenk, C. S., & White, S. D. M. 1995, MNRAS, 275, 56
Navarro, J. F., & Steinmetz, M. 1997, ApJ, 478, 13
———. 2000, ApJ, 538, 477
Peebles, P. J. E. 1969, ApJ, 155, 393
Salpeter, E. E. 1955, ApJ, 121, 161
Sandage, A., Tammann, G. A., & Yahil, A. 1979, ApJ, 232, 352 (STY79)
Schechter, P. 1976, ApJ, 203, 557
Schechter, P. L., & Dressler, A. 1987, AJ, 94, 563
Somerville, R. S., Primack, J. R., & Faber, S. M. 2001, MNRAS, 320, 504
Toomre, A. 1977, in The Evolution of Galaxies and Stellar Populations, ed. B. M. Tinsley & R. B. Larson (New Haven: Yale Univ. Press), 401
van den Bosch, F. C., Burkert, A., & Swaters, R. A. 2001, MNRAS, 326, 1205
Wadadekar, Y., Robbason, B., & Kembhavi, A. 1999, AJ, 117, 1219